Fluidization Induced by Magnetic Interactions in Confined Active Matter

Marco Musacchio,[1,2] Markus Felber,[3] Matteo Paoluzzi,[1]
Andrea Gnoli,[1,4] Andrea Puglisi,[1,4,5] and Luca Angelani[1,4]

[1]*Dipartimento di Fisica, Sapienza Università di Roma, Piazzale A. Moro 2, I-00185, Rome, Italy*
[2]*Institut für Theoretische Physik II: Weiche Materie, Heinrich-Heine-Universität Düsseldorf, Universitätsstraße 1, D-40225 Düsseldorf, Germany*
[3]*Institute of Science and Technology Austria, Am Campus 1, 3400 Klosterneuburg, Austria*
[4]*Istituto dei Sistemi Complessi - Consiglio Nazionale delle Ricerche, Piazzale A. Moro 2, I-00185, Rome, Italy*
[5]*INFN, Sezione Roma2, Via della Ricerca Scientifica 1, I-00133, Rome, Italy*

(Received 10 November 2025; accepted 30 April 2026; published 18 May 2026)

We investigate magnetic active matter in confined geometries using both experiments with magnetic toy robots, Hexbugs, and simulations of elongated magnetic active Brownian particles in circular domains. Standard active particles tend to accumulate at boundaries, forming clusters even at relatively low densities. In the presence of magnetic interactions, we provide evidence for a *fluidization* effect that inhibits clustering and shifts its onset to higher packing fractions. Moreover, magnetic dipolar interactions give rise to collective behaviors such as train-like formations, rotating pairs, and rotating clusters.

DOI: 10.1103/hylm-ljlf

I. INTRODUCTION

Originally, the passage from chaotic to ordered behavior has been investigated in molecular systems: this is what goes under the name of phase transitions and typically involves very large numbers of particles at thermodynamic equilibrium [1,2]. For decades, physicists in the field of complex systems have directed their attention to the emergence of spontaneous order in phenomena not involving molecular matter, typically violating the rules of equilibrium, because of relevant energetic transformations, such as friction and self-propulsion [3,4]. Such kinds of systems usually embrace "macroscopic molecules" such as granular and active particles. The former are passive particles which—as a consequence of their size—interact through inelastic collisions [5,6]. The latter are particles propelled by some kind of internal motor that converts stored energy into persistent motion [7,8]. Examples of active particles range from micron size, as in the case of bacteria and self-propelled colloids, to the macroscale, as in the case of fishes, birds, and robots [7,9–15].

Among a plethora of collective phenomena emerging in active matter [16,17], two of them are peculiar to the active systems we study here: accumulation at boundaries and flocking [18]. The former is related to the tendency of active particles to accumulate near confining walls, due to the persistent character of the motion [19–24], closely related to motility-induced phase separation (MIPS) [25], which occurs in the bulk. Flocking is the transition observed when aligning self-propelled particles produces polar order over large scales [26–28]. Active particles exhibiting magnetic properties are particularly intriguing [29–31], especially in biological contexts. In magnetotactic bacteria, magnetic interactions not only govern the orientation of individual cells with respect to the Earth's magnetic field, but also influence collective behavior through dipolar interactions between magnetosomes [32].

Recently, small robots such as Hexbugs nano® [33] and other similar motorized particles have been proposed as a flexible prototype for the experimental study of active matter [34–43]. They are a remarkably rich source of phenomena that can be explored in the laboratory without requiring expensive technology or specialized expertise in biological fields.

In [44], it has been shown that Hexbugs, without any magnetic interaction, can display, above a relatively small packing fraction, a drop-like clustering behavior stabilized by the hard boundary. Here, we study the interplay between boundary-induced collective phenomena and magnetic interactions in systems of Hexbugs, conducting experiments and numerical simulations.

We demonstrate that dipolar magnetic interactions inhibit boundary cluster formation, thereby increasing the critical packing fraction and leading to the emergence of new collective behaviors.

II. EXPERIMENTS

A. Experimental setup

We performed experiments with two types of elongated "particles," magnetic and nonmagnetic Hexbugs (see Fig. 1). A 3D-printed shell on both units ensures smoother contact interactions. Magneto-bugs are equipped with two small permanent neodymium magnets (cubic shape, 5 mm wide, with a magnetic moment of 0.09 A m^2) placed with their polar vector

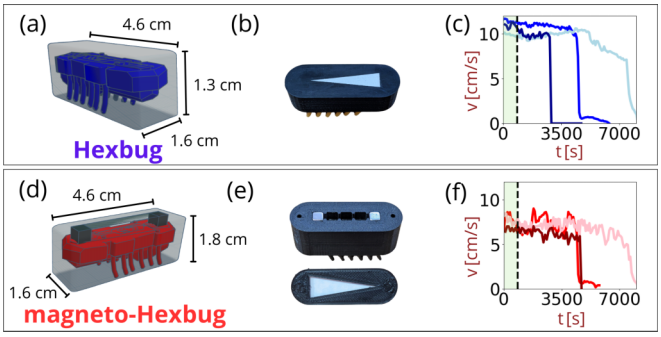

FIG. 1. Experimental setup: (a),(d) 3D models of the Hexbugs and the magneto-Hexbug. The shell of the magnetic bug is taller to accommodate two or more small neodymium magnets. (b),(e) Images of the Hexbug and the magneto-Hexbug showing their shells and the white marker used in the tracking process. (c),(f) Temporal profiles of the speed for three magnetic and three nonmagnetic particles. The green shaded areas represent the typical duration of the experiments performed.

pointing in the same direction as the main axis of the particle, one close to the head and one to the tail. Slight differences in shell weight result in variations in the characteristic speeds of the two types as reported in panels (c) and (f) of Fig. 1, where three different temporal speed profiles are shown for both the magnetic and nonmagnetic cases. Indeed, nonmagnetic bugs are lighter and therefore can express a higher speed (∼10 cm/s); magnetic bugs are heavier, resulting in a smaller speed (∼6 cm/s). Different bugs also exhibit different lifetimes; however, this does not affect the experiments performed, since their duration is typically 14 minutes and is represented by the green-shaded areas [see panels (c) and (f) in Fig. 1], during which the speed remains almost constant. We note that, while the battery lifetime is consistent with the observations reported in [44] (their Fig. S1), the speed of our Hexbugs is generally lower but more stable over time compared to that study. This discrepancy can be attributed to the specific experimental conditions under which the results in Fig. 1 were obtained: both magnetic and nonmagnetic Hexbugs were confined to a circular track to facilitate motion tracking. Nevertheless, this setup is useful to quantify, under identical conditions, the velocity ratio between the two types of particles.

We have also detected, as in all previous studies with Hexbugs [44,45], an evident tendency of the bugs to follow curve paths with each bug exhibiting a systematic curvature (in both radius and orientation) with fluctuations, not easy to be fully characterized in a finite-size arena such as ours. A population of bugs seems to contain a distribution of curvatures which is roughly symmetric around zero. We adopt for this curvature the term "chirality," in accordance with [44]. We also directly measured self-alignment [28,46,47] and incorporated it into the model to capture the full phenomenology. Our bugs have a non-negligible inertia, for instance, some bounce back can be observed in collisions with the wall or in direct collisions between two Hexbugs. However, the simulations we have performed (see the *Simulations* section), neglecting inertia, can provide us with a fair qualitative account of our main experimental observations, suggesting that it is not a crucial ingredient of the phenomenology.

The experiments involve tracking the dynamics of N (up to 39) Hexbugs within a circular arena with a diameter of 30 cm, 3D-printed in polylactic acid (PLA), with boundaries and no roof. The floor is smoothed with an adhesive polyvinyl chloride (PVC) film.

Regarding the initialization of our system, in the nonmagnetic case, all Hexbugs were placed inside a tray that tightly fits three rows of 13 bugs; after all bugs are switched on, the tray is lifted; the bugs in one row are all oriented toward another row, causing them to immediately break up any order and diffuse into the arena. A different strategy was adopted in the magnetic experiments: due to magnetic interactions, initializing the bugs in a compact configuration would have delayed the system's relaxation toward its final state. In this case, the magneto-Hexbugs were allowed to enter the arena one by one through an external railway, and the experiment effectively started once all the selected bugs were inside the arena. Moreover, to ensure that the experiments were not affected by a drop in the battery life of some Hexbugs, we tracked each bug's hours of activity and replaced the batteries so as to avoid observing a sudden decrease in the particles' speed.

B. Experimental results

The main experimental results are recapitulated in Fig. 2 (see Supplemental Material [48]). Following the terminology of [44], we observe "boundary polar clusters" in both magnetic and nonmagnetic cases, provided that the number of particles is large enough, see Figs. 2(b), 2(c), and 2(f). These clusters are characterized by a majority of particles with aligned polar vectors—pointing roughly perpendicular to the boundary and toward the outside of the arena—and close-packed positions along the boundary. All clusters display two "confining" particles at their extremes, which push inward, providing stability of the cluster. Variations of this typical arrangement include the presence of defects [see Fig. 2(c)] as well as multilayering [see Fig. 2(f)]. For small numbers of particles, the clusters do not form, and the particles are typically found moving along trajectories which are (roughly) parallel to the boundary: in the case of nonmagnetic particles, this "gas" phase is without an evident positional order, while in the magnetic case, the particles typically display "trains" of variable length, not far from the boundary. The formation of these "trains" is characteristic of dipolar interactions, and the lengths of these structures range from just two particles up to a number comparable to the total number of Hexbugs in the arena. These structures are stable for a limited time before breaking down and possibly reforming. We observe that, in the low-density regime, boundary-following trajectories tend to exhibit *antichirality*, moving in the direction opposite to the intrinsic chirality of unconfined Hexbug particles. This occurs because chiral motion more effectively stabilizes boundary trajectories with opposite chirality.

The main difference between the nonmagnetic and magnetic cases, which represents our main experimental observation, is the increase of the clustering threshold density for the magnetic particles. This result is made clear in Figs. 2(g)

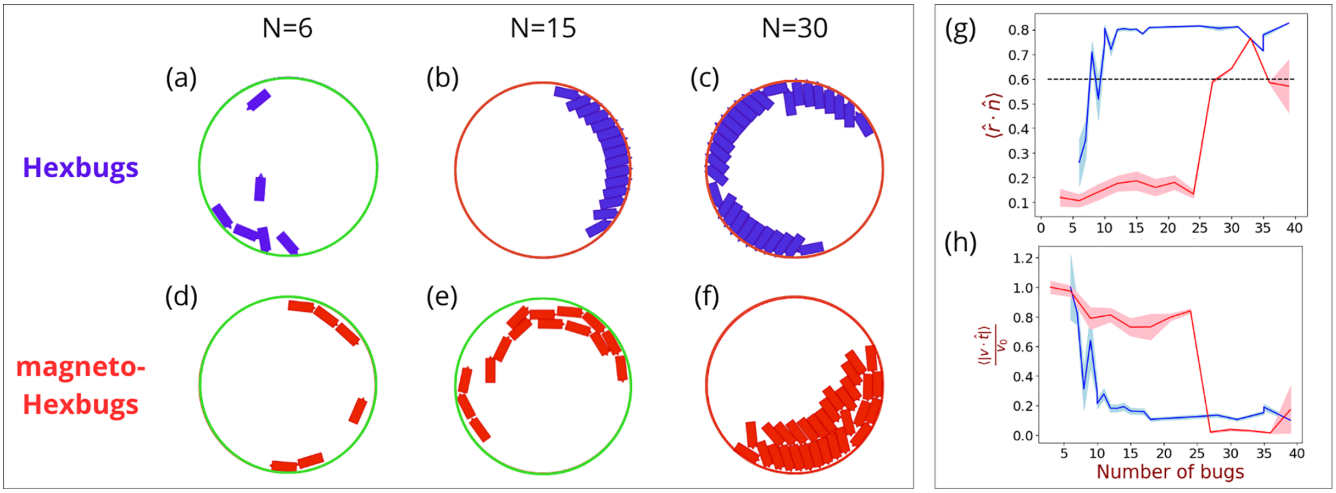

FIG. 2. Experimental results: (a)–(c) Experimental frames showing the final configurations for $N = 6, 15,$ and 30 Hexbugs. (d)–(f) Experimental frames showing the final configurations for $N = 6, 15,$ and 30 magneto-Hexbugs. (g) Plot of $\langle \hat{r} \cdot \hat{n} \rangle$, where $\hat{r}$ is the unit vector pointing from the arena center to the particle's center of mass, and $\hat{n}$ is the unit vector of the particle's orientation. (h) Plot of $\langle |v \cdot \hat{t}| \rangle / v_0$, where $\hat{t}$ is the unit vector perpendicular to $\hat{r}$ (i.e., locally tangent to the boundary), v is the particle velocity, and v_0 is the mean velocity measured at the lowest density. The shaded areas in panels (g) and (h) represent the errors associated with the order parameters. Blue curve: experiments with Hexbugs; red curve: experiments with magneto-Hexbugs. Green and red boundaries in (a)–(f) are used to highlight the final configuration, without or with boundary clusters, respectively.

and 2(h), where two different order parameters are shown as a function of the number of particles, for the nonmagnetic (blue data) and magnetic (red data) particles. In Fig. 2(g), we show $\langle \hat{r} \cdot \hat{n} \rangle$, where $\hat{r}$ is the unit vector of the center of mass position of each particle, assuming the center of the arena as the origin, while $\hat{n}$ is the unit vector representing the polar orientation of each particle. The scalar product is first averaged over all particles at a given time, and then averaged over a long realization of the experiment (corresponding to about two-thirds of the total duration, i.e., approximately 10 minutes).

The figure shows a clear transition in the order parameter from a majority of particles aligned to the boundary ($\langle \hat{r} \cdot \hat{n} \rangle \approx 0.1$) to a majority of particles perpendicular to it ($\langle \hat{r} \cdot \hat{n} \rangle \gtrsim 0.6$), signaling the emergence of polar boundary clusters. The transition occurs at $N = N^*_{nm} \approx 10$ for nonmagnetic particles and at $N = N^*_m \approx 27$ for magnetic ones.

The other order parameter we have analyzed is $\langle |v \cdot \hat{t}| \rangle / v_0$, where $\hat{t}$ is the unit vector perpendicular to $\hat{r}$, i.e., parallel to the boundary in the proximity of the particle, and v is the velocity vector of the particle (where v_0 denotes the mean velocity observed at the lowest density). This order parameter signals the same transition—from ~ 1 (particles moving parallel to the boundary) to ~ 0 (particles not moving or moving perpendicular to it)—at the same critical sizes $N^*_{nm} < N^*_m$. This order parameter is related to velocity instead of orientation: it may appear that the two are usually parallel, but this is not true at high density, e.g., in the cluster phase, and in fact, it is seen that a residual velocity parallel to the boundary is observed. The clusters crawl along the boundary thanks to a small asymmetry in their internal structure, at a speed which is significantly lower than the free speed of particles. We highlight that the choice of two orientational order parameters is motivated by the fact that boundary clusters appear only when the particles are oriented perpendicular to the boundary.

We also note the emergence of several characteristic transient structures during the dynamic evolution of magnetic Hexbugs, such as rotating pairs, linear trains, and rotating clusters composed of three or more particles (see Fig. 3), never observed in nonmagnetic bugs.

III. SIMULATIONS

A. Simulation model

Numerical simulations are performed considering N active Brownian particles with an elongated shape and confined in a 2D circular domain. Each particle i is described by its center of mass position $\mathbf{r}_i$, orientation $\hat{\mathbf{n}}_i = (\cos(\varphi_i), \sin(\varphi_i))$, and $M = 5$ centers of force along its principal axis, whose positions are $\mathbf{r}_i^\alpha$ ($\alpha = 1, \ldots, M$).

Magnetic particles are equipped with two magnets with magnetic moment $\mathbf{m}_i = m\hat{\mathbf{u}}_i$, whose orientation coincides with the particle's orientation $\hat{\mathbf{u}}_i = \hat{\mathbf{n}}_i$ (but in general could be

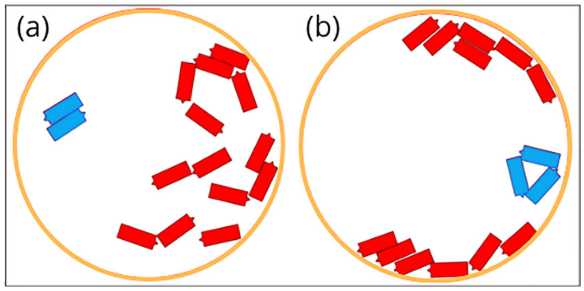

FIG. 3. Typical rotating structures (blue particles) observed in experiments resulting from dipole–dipole magnetic interactions: (a) a rotating pair and (b) a three-particle rotating cluster.

different), and position $\mathbf{r}_i^p$ ($p = 1, 2$). The equations of motion of the i-th particle in the overdamped regime are

$$\gamma \dot{\mathbf{r}}_i = -\nabla_i U + \mathbf{F}_{i,active}, \tag{1}$$

$$\gamma_r \dot{\varphi}_i = \mathbf{T}_i \cdot \hat{\mathbf{z}} + \beta\,(\hat{\mathbf{n}}_i \times \dot{\mathbf{r}}_i) \cdot \hat{\mathbf{z}} + \gamma_r \eta, \tag{2}$$

where γ and γ_r are the translational and rotational friction coefficients, $\mathbf{F}_{i,active} = \gamma v_0 \hat{\mathbf{n}}_i$ is the self-propulsion force of each unit (v_0 is the self-propelled speed), β is the strength of the self-alignment term [46], and η is a Gaussian white noise with zero mean $\langle \eta(t) \rangle = 0$ and variance $\langle \eta(t)\eta(s) \rangle = 2D_r\delta(t - s)$, with D_r the rotational diffusion constant. The potential energy $U = \sum_{i<j}(\sum_{\alpha,\beta} U_{\mathrm{S}}(r_{ij}^{\alpha\beta}) + \sum_{p,q} U_{\mathrm{M}}(\mathbf{r}_{ij}^{pq}, \hat{\mathbf{u}}_i, \hat{\mathbf{u}}_j))$ accounts for both steric interactions and dipole–dipole interactions. In the previous expression, the sum on α, β runs over centers of force and the sum on p, q over magnets of each particle, $\mathbf{r}_{ij}^{\alpha\beta} = \mathbf{r}_i^{\alpha} - \mathbf{r}_j^{\beta}$, $r_{ij}^{\alpha\beta} = |\mathbf{r}_{ij}^{\alpha\beta}|$, and similarly for $\mathbf{r}_{ij}^{pq}$. The steric term is a truncated repulsive soft potential, $U_{\mathrm{S}}(r) = 4\varepsilon(\sigma/r)^{12}\,\theta(r_c - r)$, where (ϵ, σ) set the energy and length scales of the interaction, σ is the diameter of the particles, r_c is a cutoff radius, and θ is the Heaviside step function. The magnetic interactions are described by the dipole–dipole energy

$$U_{\mathrm{M}}(\mathbf{r}, \hat{\mathbf{u}}_1, \hat{\mathbf{u}}_2) = \frac{\mu_0 m^2}{4\pi r^3}\left[\hat{\mathbf{u}}_1 \cdot \hat{\mathbf{u}}_2 - 3\frac{(\hat{\mathbf{u}}_1 \cdot \mathbf{r})(\hat{\mathbf{u}}_2 \cdot \mathbf{r})}{r^2}\right]. \tag{3}$$

The boundary-particle interaction is modeled using the image particle method [49–51].

$\mathbf{T}_i$ represents the torque that arises from both steric and dipole–dipole interactions, while the term $\beta\,(\hat{\mathbf{n}}_i \times \dot{\mathbf{r}}_i)$ is an additional torque that forces the particle to align its orientation with its velocity. This term is referred to as self-alignment and arises from the displacement of the center of friction with respect to the center of mass of the particle [46].

More specifically, in order to correctly compute the torque T_i appearing in Eq. (2), we have considered three different contributions. The first one arises from steric interactions, which are computed for all the M centers of force along the principal axes of each particle and subsequently added to the evolution of the particle's orientation. The other contributions originate from magnetic interactions. Considering two magnetic dipoles belonging to different particles located at positions $\mathbf{r}_i^p$ and $\mathbf{r}_j^q$, the magnetic field produced by magnet q of particle j on the magnet p of particle i is $\mathbf{B}(\mathbf{r}_{ij}^{pq}, \hat{\mathbf{u}}_j)$, where $\mathbf{r}_{ij}^{pq} = \mathbf{r}_i^p - \mathbf{r}_j^q$, $\hat{\mathbf{u}}_j$ is the orientation of the magnet q of particle j and

$$\mathbf{B}(\mathbf{r}, \hat{\mathbf{u}}) = \frac{\mu m}{4\pi r^3}\left[\frac{3\mathbf{r}(\mathbf{r} \cdot \hat{\mathbf{u}})}{r^2} - \hat{\mathbf{u}}\right]. \tag{4}$$

The torque exerted on particle i by the magnets of particle j can be expressed as

$$\mathbf{T}_{ij} = \sum_{p,q} m\hat{\mathbf{u}}_i \times \mathbf{B}\big(\mathbf{r}_{ij}^{pq}, \hat{\mathbf{u}}_j\big). \tag{5}$$

The second contribution to the torque due to magnetic interactions arises from the fact that the magnetic forces governing the translational dynamics described in Eq. (1) are applied not at the particle's center of mass, but at the center of the magnet.

The majority of the parameters used in the simulations are fixed by experimental observations, such as the dipole strength and the position of the magnets inside the magneto-Hexbugs shell, the particle and arena dimensions, particles' velocities, and the translational friction coefficient. After establishing the values of these parameters, we conducted a careful and targeted search for the remaining parameters, adjusting them to more closely match the experimental results, in particular the spatial structures and the order parameters as a function of N. Even if the number of parameters is large, our requirement of obtaining the full phenomenology with two main phases at different values of N puts a severe constraint.

In particular, we choose them such that the Péclet number, $\mathrm{Pe} = v_0/(D_r\sigma)$, takes the value $\mathrm{Pe} = 70$ for nonmagnetic Hexbugs and $\mathrm{Pe} = 50$ for magnetic ones. In both cases, the speed distributions are modeled as truncated Gaussian distributions, the dimensionless strength of the magnetic interaction is $\Lambda = \mu_0 m^2/(4\pi\,\sigma^3\,D_r\gamma_r) = 7.13$, the reduced self-alignment strength is $B = \beta\sigma/\gamma_r = 0.35$, and the dimensionless friction ratio is $\gamma/(\sigma^2\gamma_r) = 1/6$.

To test cluster stability, the system was initialized in a preassembled configuration and then allowed to evolve as already done in [44].

B. Simulation results

The results of the simulations are shown in Fig. 4 (see Supplemental Material [48]), which represents the numerical counterpart of the experimental results of Fig. 2. We first notice that the observed configurations are quite similar to the experimental ones, with the exception of a lack of defects in the boundary clusters of the nonmagnetic case. All other observations, such as trains in the low-density magnetic system, single layers of boundary clusters in the nonmagnetic case, opposed to bilayers in the magnetic one, are faithfully reproduced.

The behavior with N of the two aforementioned order parameters is also in fair agreement with the experiments, with transitions from nonclustered to clustered phases at $N_{nm}^* < N_m^*$ with values compatible with the experiments. We note that in the simulation, the transition of the nonmagnetic system is less sharp, i.e., the growth of the order parameter is smoother and, in particular, for $\langle \hat{r} \cdot \hat{n} \rangle$, it does not immediately saturate for values $N \gtrsim N_{nm}^*$.

To enable a more detailed comparison between experiments and simulations in the magnetic case, Fig. 5 presents the velocity distributions [Figs. 5(a) and 5(b)], as well as the distributions of the relative angle between particle orientation and position vector, $\phi = \cos^{-1}(\hat{\mathbf{n}} \cdot \hat{\mathbf{r}})$, for 6, 15, and 30 bugs [Figs. 5(c)–5(e)]. Panels (a) and (b) show that, in both simulations and experiments, increasing system density leads to a shift in the velocity distribution toward lower values, consistent with the formation of particle clusters. Panels (c)–(e) demonstrate that magneto-Hexbugs at low densities predominantly move parallel to the boundary (indicated by a peak near $\pi/2$). As N increases, the emergence of clusters with radially oriented particles results in angle distributions shifting toward zero. The small peak near $\pi/2$ observed at $N = 30$ indicates

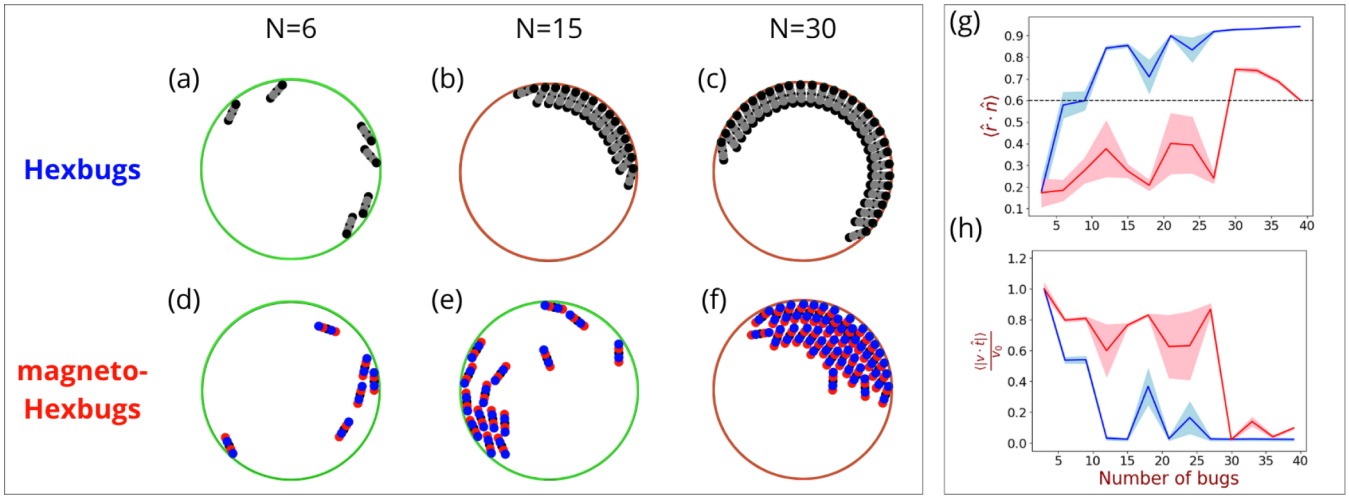

FIG. 4. Simulation results: (a)–(c) Simulation frames showing the final configurations for $N = 6$, 15, and 30 particles. (d)–(f) Simulation frames showing the final configurations for $N = 6$, 15, and 30 magnetic particles. In all cases (a)–(f), each Hexbug is represented by its five centers of force, depicted as colored discs (gray and black for the nonmagnetic, red and blue for the magnetic ones); the head of a Hexbug is the only disk which is fully visible (black for the nonmagnetic, blue for the magnetic ones). (g) Plot of $\langle \hat{r} \cdot \hat{n} \rangle$, where $\hat{r}$ is the unit vector pointing from the arena center to the particle's center of mass, and $\hat{n}$ is the unit vector of the particle's orientation. (h) Plot of $\langle |v \cdot \hat{t}| \rangle / v_0$, where $\hat{t}$ is the unit vector perpendicular to $\hat{r}$ (i.e., locally tangent to the boundary), v is the particle velocity, and v_0 is the mean velocity measured at the lowest density. The shaded areas in panels (g) and (h) represent the errors associated with the order parameters. Blue curve: simulations with nonmagnetic particles; red curve: simulations with magnetic particles.

that some particles within the cluster maintain alignment with the boundary.

IV. CONCLUSIONS

We investigated magnetically active systems by conducting experiments with modified Hexbug toy robots, each equipped with a shell containing small permanent magnets. We discovered that magnetic interactions produce a *fluidization* effect, meaning that they can postpone, in terms of particle density, the formation of stable boundary clusters. More specifically, we found that boundary clusters form at higher densities with respect to the nonmagnetic case and are possible only when the particles are oriented perpendicular to the boundary. The transition from a nonclustered state to a clustered one is studied through two order parameters that highlight the formation of polar clusters with vanishing tangential velocity. The increase of the critical density required for cluster formation in the magnetic case may be partially attributed to the reduced mean velocity of the magnetic robots (Pe $\sim$ 50) compared to the nonmagnetic ones (Pe $\sim$ 70). However, such a shift is expected to be on the order of $\sim$20% in the critical density [44], whereas the experimentally measured variation is approximately 170% of the nonmagnetic critical density. This significant discrepancy therefore provides evidence of the additional contribution of dipolar interactions to the observed fluidization effect.

Furthermore, magnetic interactions produce a wide variety of particular transient configurations, such as train-like structures, rotating pairs, and rotating clusters. We confirmed these results through numerical simulations, implementing a model of active magnetic particles that reproduced the experimental conditions, finding very good agreement between them. Both the fluidization effect and the transient configurations observed in the presence of magnetic interactions are possible in a range where the magnetic force between two dipoles is comparable to the active force. This ensures that bulk clusters dominated by magnetic interactions do not form when the magnets are too strong, while also preventing the disappearance of the previously described effects when the magnetic strength is too low.

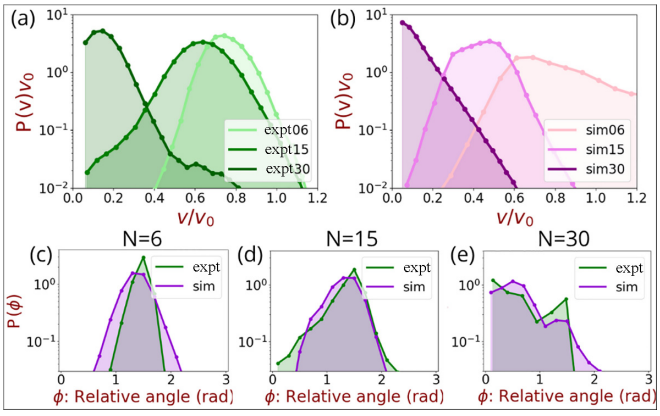

FIG. 5. Comparison between experiments and simulations for magneto-Hexbugs. (a),(b) Velocity distributions for $N = 6$, 15, and 30 bugs in experiments (a) and simulations (b). Velocities are normalized by v_0, defined as the typical body length of a Hexbug divided by the characteristic time it takes to travel this distance. (c)–(e) Probability distributions of the relative angle ϕ (modulo π), shown in green for experiments and violet for simulations. The angle ϕ is defined as the difference between the particle orientation in the laboratory frame and the angle of the vector from the arena center to the particle's center of mass. The cases with N = 6, 15, and 30 are shown.

We remark that we managed to obtain a good agreement between experiments and simulations even without chirality (we mention the fact that self-alignment was not considered in [44] and in the same work chirality was observed to inhibit clustering and polar ordering). On the contrary, we have realized that a crucial ingredient is the distribution of particle speeds, motivated by the variability in the bugs' speeds reported in panels (c) and (f) of Fig. 1; otherwise, certain structures (such as boundary-running trains) are too stable and never break in favor of clusters. The speed distribution that we found to be optimal for comparison with experiments is a Gaussian distribution with two thresholds, in order to avoid having bugs that are too slow or too fast. The mean value of the Gaussian distribution is 0.7 for the nonmagnetic-Hexbugs and 0.5 for the magnetic ones, for which the resulting ratio is consistent with the experimental data reported in Fig. 1.

Finally, we underline that we observe a transition from a disordered "gas-like" phase to a boundary-clustered phase, without coexistence. This is coherent with the claim, in [44], that phase coexistence requires inertia and that in the overdamped limit, the same adopted in our numerical study, their simulations display pure clusters at the boundaries (their Fig. S7).

An intriguing question is whether this *fluidization* effect persists in bulk systems, potentially influencing the MIPS phenomenon [52]. Furthermore, our design enables the systematic study of various magnetic particle configurations, allowing for controlled modifications in the position, number, and orientation of the magnets. This flexibility opens the door to exploring a broad range of interaction scenarios and collective behaviors in magnetic active matter.

ACKNOWLEDGMENTS

The authors acknowledge discussions with Lorenzo Caprini. A.G., M.P., and A.P. acknowledge funding from the Italian Ministero dell'Università e della Ricerca under the program PRIN 2022 ("Re-ranking of the final lists"), Grants No. 2022KWTEB7 with CUP No. B53C24006470006. L.A. acknowledges funding from the Italian Ministero dell'Università e della Ricerca under the program PRIN 2020, Grant No. 2020PFCXPE.

DATA AVAILABILITY

The data that support the findings of this article are not publicly available upon publication because it is not technically feasible and/or the cost of preparing, depositing, and hosting the data would be prohibitive within the terms of this research project. The data are available from the authors upon reasonable request.

[1] M. Toda, R. Kubo, and N. Saito, *Statistical Physics I: Equilibrium Statistical Mechanics*, 2nd ed. (Springer, Berlin, Heidelberg, New York, 1978).

[2] S.-K. Ma, *Statistical Mechanics* (World Scientific Publishing Company, 1985).

[3] W. Van Saarloos, V. Vitelli, and Z. Zeravcic, *Soft Matter: Concepts, Phenomena, and Applications* (Princeton University Press, 2024).

[4] A. Sarracino, A. Puglisi, and A. Vulpiani, *Nonequilibrium Statistical Mechanics: Basic Concepts, Models and Applications* (IOP Publishing, 2025).

[5] N. V. Brilliantov and T. Pöschel, *Kinetic Theory of Granular Gases* (Oxford University Press, 2010).

[6] A. Puglisi, *Transport and Fluctuations in Granular Fluids: From Boltzmann Equation to Hydrodynamics, Diffusion and Motor Effects* (Springer, 2014).

[7] C. Bechinger, R. Di Leonardo, H. Löwen, C. Reichhardt, G. Volpe, and G. Volpe, Active particles in complex and crowded environments, Rev. Mod. Phys. **88**, 045006 (2016).

[8] M. C. Marchetti and R. A. Simha, Hydrodynamics of soft active matter, Rev. Mod. Phys. **85**, 1143 (2013).

[9] M. Ballerini, N. Cabibbo, R. Candelier, A. Cavagna, E. Cisbani, I. Giardina, V. Lecomte, A. Orlandi, G. Parisi, A. Procaccini, M. Viale, and V. Zdravković, Interaction ruling animal collective behavior depends on topological rather than metric distance: Evidence from a field study, Proc. Natl. Acad. Sci. USA **105**, 1232 (2008).

[10] C. Scholz, M. Engel, and T. Pöschel, Rotating robots move collectively and self-organize, Nat. Commun. **9**, 931 (2018).

[11] M. Workamp, G. Ramirez, K. E. Daniels, and J. A. Dijksman, Symmetry-reversals in chiral active matter, Soft Matter **14**, 5572 (2018).

[12] F. Siebers, A. Jayaram, P. Blümler, and T. Speck, Exploiting compositional disorder in collectives of light-driven circle walkers, Sci. Adv. **9**, eadf5443 (2023).

[13] L. Caprini, D. Breoni, A. Ldov, C. Scholz, and H. Löwen, Dynamical clustering and wetting phenomena in inertial active matter, Commun. Phys. **7**, 343 (2024).

[14] G. Volpe, N. A. Araújo, M. Guix, M. Miodownik, N. Martin, L. Alvarez, J. Simmchen, R. Di Leonardo, N. Pellicciotta, Q. Martinet, *et al.*, Roadmap for animate matter, J. Phys.: Condens. Matter **37**, 333501 (2025).

[15] A. P. Antonov, M. Musacchio, H. Löwen, and L. Caprini, Self-sustained frictional cooling in active matter, Nat. Commun. **16**, 7235 (2025).

[16] M. J. Bowick, N. Fakhri, M. C. Marchetti, and S. Ramaswamy, Symmetry, thermodynamics, and topology in active matter, Phys. Rev. X **12**, 010501 (2022).

[17] J. Elgeti, R. G. Winkler, and G. Gompper, Physics of microswimmers—single particle motion and collective behavior: a review, Rep. Prog. Phys. **78**, 056601 (2015).

[18] T. Vicsek, A. Czirók, E. Ben-Jacob, I. Cohen, and O. Shochet, Novel type of phase transition in a system of self-driven particles, Phys. Rev. Lett. **75**, 1226 (1995).

[19] G. Li and J. X. Tang, Accumulation of microswimmers near a surface mediated by collision and rotational Brownian motion, Phys. Rev. Lett. **103**, 078101 (2009).

[20] J. Elgeti and G. Gompper, Wall accumulation of self-propelled spheres, Europhys. Lett. **101**, 48003 (2013).

[21] J. Elgeti and G. Gompper, Run-and-tumble dynamics of self-propelled particles in confinement, Europhys. Lett. **109**, 58003 (2015).
[22] H. H. Wensink and H. Löwen, Aggregation of self-propelled colloidal rods near confining walls, Phys. Rev. E **78**, 031409 (2008).
[23] L. Angelani, Confined run-and-tumble swimmers in one dimension, J. Phys. A: Math. Theor. **50**, 325601 (2017).
[24] L. Angelani, One-dimensional run-and-tumble motions with generic boundary conditions, J. Phys. A: Math. Theor. **56**, 455003 (2023).
[25] J. Tailleur and M. E. Cates, Statistical mechanics of interacting run-and-tumble bacteria, Phys. Rev. Lett. **100**, 218103 (2008).
[26] J. Toner and Y. Tu, Long-range order in a two-dimensional dynamical XY model: How birds fly together, Phys. Rev. Lett. **75**, 4326 (1995).
[27] M. Paoluzzi, D. Levis, and I. Pagonabarraga, From flocking to glassiness in dense disordered polar active matter, Commun. Phys. **7**, 57 (2024).
[28] M. Musacchio, A. P. Antonov, H. Löwen, and L. Caprini, Flocking as a second-order phase transition in self-aligning active crystals, arXiv:2506.12967.
[29] S. H. L. Klapp, Collective dynamics of dipolar and multipolar colloids: From passive to active systems, Current Opinion in Colloid & Interface Science **21**, 76 (2016).
[30] A. Compagnie, N. Vandewalle, and E. Opsomer, Magnetically assisted trapping of passive colloids by active dipolar chains, arXiv:2509.13770.
[31] M. Rosenberg and H. Löwen, Windmilling clusters of active quadrupoles, J. Chem. Phys. **164**, 084901 (2026).
[32] M. Marmol, E. Gachon, and D. Faivre, *Colloquium*: Magnetotactic bacteria: From flagellar motor to collective effects, Rev. Mod. Phys. **96**, 021001 (2024).
[33] https://www.hexbug.com/nano.html.
[34] A. Barona Balda, A. Argun, A. Callegari, and G. Volpe, Playing with active matter, Am. J. Phys. **92**, 847 (2024).
[35] O. Dauchot and V. Démery, Dynamics of a self-propelled particle in a harmonic trap, Phys. Rev. Lett. **122**, 068002 (2019).
[36] M. Leoni, M. Paoluzzi, S. Eldeen, A. Estrada, L. Nguyen, M. Alexandrescu, K. Sherb, and W. W. Ahmed, Surfing and crawling macroscopic active particles under strong confinement: Inertial dynamics, Phys. Rev. Res. **2**, 043299 (2020).
[37] A. Escobar, R. Reyes-Aguilar, C. Vidales-Hernández, J. Carrillo-Estrada, and F. Donado, Effect of particle concentration on the persistence of motion in active matter systems, Physica A **659**, 130344 (2025).
[38] L. Ning, H. Zhu, J. Yang, Q. Zhang, P. Liu, R. Ni, and N. Zheng, Macroscopic, artificial active matter, National Science Open **3**, 20240005 (2024).
[39] N. Vanesse, E. Opsomer, G. Lumay, and N. Vandewalle, Collective dynamics of dipolar self-propelled particles, Phys. Rev. E **108**, 024608 (2023).
[40] N. Sepúlveda, F. Guzmán-Lastra, M. Carrasco, B. González, E. Hamm, and A. Concha, Bioinspired magnetic active matter and the physical limits of magnetotaxis, arXiv:2111.04889 [cond-mat.soft].
[41] P. M. Obreque, O. Garrido, D. Romero, H. Löwen, and F. Guzmán-Lastra, Dynamics of magnetic self-propelled particles in a harmonic trap, arXiv:2403.02569 [cond-mat.soft].
[42] O. Chor, A. Sohachi, R. Goerlich, E. Rosen, S. Rahav, and Y. Roichman, Many-body Szilárd engine with giant number fluctuations, Phys. Rev. Res. **5**, 043193 (2023).
[43] J. P. Carrillo-Mora, A. Garcés, and D. Levis, Depinning and activated motion of chiral self-propelled robots, Phys. Rev. E **112**, 065417 (2025).
[44] A. Deblais, T. Barois, T. Guerin, P.-H. Delville, R. Vaudaine, J. S. Lintuvuori, J.-F. Boudet, J.-C. Baret, and H. Kellay, Boundaries control collective dynamics of inertial self-propelled robots, Phys. Rev. Lett. **120**, 188002 (2018).
[45] S. van Kesteren, L. Alvarez, S. Arrese-Igor, A. Alegria, and L. Isa, Self-propelling colloids with finite state dynamics, Proc. Natl. Acad. Sci. USA **120**, e2213481120 (2023).
[46] P. Baconnier, O. Dauchot, V. Démery, G. Düring, S. Henkes, C. Huepe, and A. Shee, Self-aligning polar active matter, Rev. Mod. Phys. **97**, 015007 (2025).
[47] M. Musacchio, A. P. Antonov, H. Löwen, and L. Caprini, Self-alignment and anti-self-alignment suppress motility-induced phase separation in active systems, J. Chem. Phys. **162**, 244902 (2025).
[48] See Supplemental Material at http://link.aps.org/supplemental/10.1103/hylm-ljlf for Supplemental Videos 1 and 2 for recordings of the experiments and Supplemental Videos 3 and 4 for simulation results.
[49] L. Angelani, R. Di Leonardo, and G. Ruocco, Self-starting micromotors in a bacterial bath, Phys. Rev. Lett. **102**, 048104 (2009).
[50] M. Paoluzzi, R. Di Leonardo, and L. Angelani, Self-sustained density oscillations of swimming bacteria confined in microchambers, Phys. Rev. Lett. **115**, 188303 (2015).
[51] M. Paoluzzi, L. Angelani, and A. Puglisi, Narrow-escape time and sorting of active particles in circular domains, Phys. Rev. E **102**, 042617 (2020).
[52] G. Spera, C. Duclut, M. Durand, and J. Tailleur, Nematic torques in scalar active matter: When fluctuations favor polar order and persistence, Phys. Rev. Lett. **132**, 078301 (2024).